JOURNAL OF GEOPHYSICAL RESEARCH, VOL. 114, B10310, doi:10.1029/2009JB006307, 2009

Composition and variation of noise recorded at the Yellowknife Seismic Array, 1991–2007

Keith D. Koper,[1] Benjamin de Foy,[1] and Harley Benz[2]

Received 14 January 2009; revised 22 June 2009; accepted 3 August 2009; published 17 October 2009.

[1] We analyze seismic noise recorded on the 18 short-period, vertical component seismometers of the Yellowknife Seismic Array (YKA). YKA has an aperture of 23 km and is sited on cratonic lithosphere in an area with low cultural noise. These properties make it ideal for studying natural seismic noise at periods of 1–3 s. We calculated frequency-wave number spectra in this band for over 6,000 time windows that were extracted once per day for 17 years (1991–2007). Slowness analysis reveals a rich variety of seismic phases originating from distinct source regions: R_g waves from the Great Slave Lake; L_g waves from the Atlantic, Pacific, and Arctic Oceans; and teleseismic P waves from the north Pacific and equatorial mid-Atlantic regions. The surface wave energy is generated along coastlines, while the body wave energy is generated at least in part in deep-water, pelagic regions. Surface waves tend to dominate at the longer periods and, just as in earthquake seismograms, L_g is the most prominent arrival. Although the periods we study are slightly shorter than the classic double-frequency microseismic band of 4–10 s, the noise at YKA has clear seasonal behavior that is consistent with the ocean wave climate in the Northern Hemisphere. The temporal variation of most of the noise sources can be well fit using just two Fourier components: yearly and biyearly terms that combine to give a fast rise in microseismic power from mid-June through mid-October, followed by a gradual decline. The exception is the R_g energy from the Great Slave Lake, which shows a sharp drop in noise power over a 2-week period in November as the lake freezes. The L_g noise from the east has a small but statistically significant positive slope, perhaps implying increased ocean wave activity in the North Atlantic over the last 17 years.

Citation: Koper, K. D., B. de Foy, and H. Benz (2009), Composition and variation of noise recorded at the Yellowknife Seismic Array, 1991–2007, *J. Geophys. Res.*, *114*, B10310, doi:10.1029/2009JB006307.

1. Introduction

[2] Primarily because of two factors there has recently been an increase of interest in Earth's seismic noise field. First is the recognition that ambient seismic noise can be used to image shallow Earth structure [*Courtland*, 2008]. Tomographers are now able to fill in gaps created by irregularities in earthquake location and produce more uniform images of wave speed variations in the crust [e.g., *Shapiro et al.*, 2005; *Sabra et al.*, 2005]. However, the theory behind this technique presupposes a diffuse symmetric noise field and if anisotropy exists in the noise then the resulting Green's functions may be biased. Currently, this problem is addressed by averaging over a year's worth of data to mitigate seasonal patterns in noise, and/or by averaging the causal and acausal portions of the cross-correlelograms. Precise location of noise sources would reduce the need for these actions and enhance temporal monitoring of Earth structure.

[3] A second factor responsible for increased interest in seismic noise is the recognition that historical records of microseisms can be used as proxies for ocean wave climate, and so perhaps have implications for understanding the effects of global warming [*Bromirski et al.*, 1999]. For instance, *Grevemeyer et al.* [2000] used a 40-year record of noise from a seismometer in Hamburg, Germany to study the wave climate in the North Atlantic. They found evidence for a strong increase in wave activity over the period of 1974–1998 that tracked increased surface air temperature in the region. More recently, *Aster et al.* [2008a] studied seismic noise recorded by 11 globally distributed seismometers over the period of 1986–2006 and found a strong annual signal at nearly all stations, as well as a signal for the El Nino event of 1997–1998. Importantly, these authors also found evidence for increased global storm activity for the period of 1972–2008 [*Aster et al.*, 2008b]. Proper location of microseism source areas can enhance these types of studies since climate change likely affects not just the number and strength of storms but also their geographical tracks.

[1]Department of Earth and Atmospheric Sciences, Saint Louis University, St. Louis, Missouri, USA.
[2]National Earthquake Information Center, United States Geological Survey, Denver, Colorado, USA.

0148-0227/09/2009JB006307$09.00

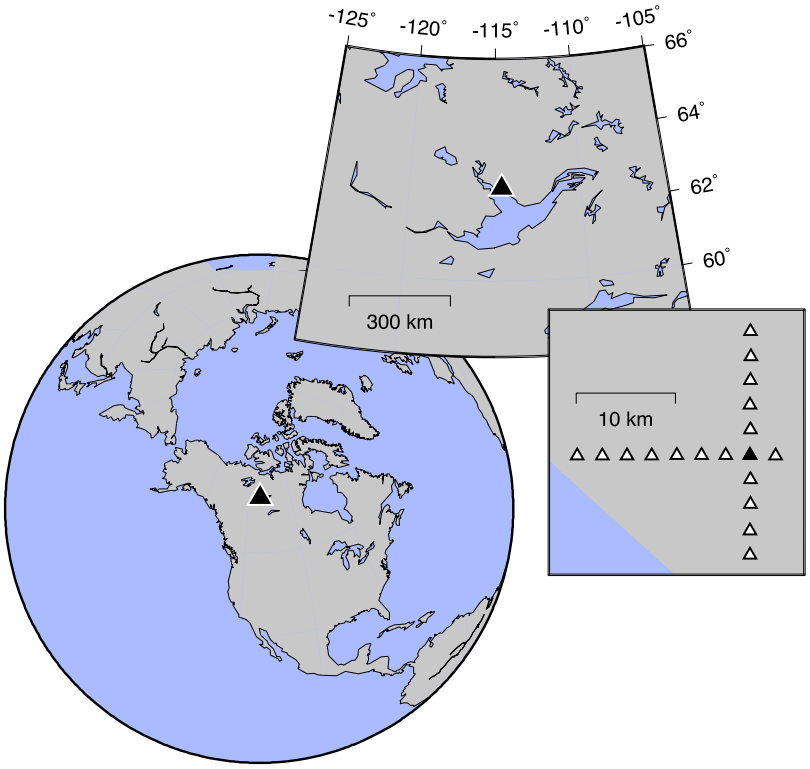

Figure 1. Geometry and location of the Yellowknife seismic array (YKA). The darkened triangle is the reference element of the array. The large body of water south of the array is the Great Slave Lake.

[4] Seismic arrays are particularly useful in studying seismic noise because they give directional constraints (backazimuth and apparent velocity) on incoming energy. This enables *P* waves to be identified and separated from surface waves, and backprojected to specific source areas [*Haubrich and McCamy*, 1969]. In fact, using continuous body wave data from modern seismic arrays enables noise sources to be geographically tracked as a function of time [*Gerstoft et al.*, 2006]. It is more difficult to locate noise sources with surface waves because at a given period they arrive with a fixed apparent velocity and so give no indication of distance. However, by considering the dispersion characteristics of water waves [*Friedrich et al.*, 1998] or by using the intersection of backazimuth estimates from more than one array [*Cessaro*, 1994] locations can be inferred. It is currently debated whether the surface wave component of microseisms observed at continental sites is generated primarily along coastlines [*Bromirski et al.*, 1999; *Bromirski*, 2001; *Bromirski et al.*, 2005; *Yang and Ritzwoller*, 2008] or if it is also generated in deep-sea areas [*Cessaro*, 1994; *Stehly et al.*, 2006; *Chevrot et al.*, 2007; *Kedar et al.*, 2008].

[5] In this work we analyze the seismic noise recorded by the Yellowknife seismic array (YKA) in northern Canada. We concentrate on locating the noise sources that are stable over long time periods and determining the type of seismic waves that they generate. Although the short-period YKA sensors are most sensitive to energy at periods of 1 s, and the dominant double-frequency band of microseismic energy occurs at periods of 4–10 s, previous work with a similar seismic array in Thailand was successful in identifying ocean-wave induced seismic energy at short periods [*Koper and de Foy*, 2008]. YKA is located on cratonic lithosphere in a remote area with low cultural noise (Figure 1), and is positioned to record microseisms from the Atlantic, Pacific, and Arctic Oceans. Because of the simple geology in the region the slowness anomalies at YKA are extremely small [*Bondar et al.*, 1999]. In practical terms this means that body wave energy observed at YKA can be accurately backprojected to geographical source regions. Digital data from YKA are available from 1991 through the present, making it one of the longest publicly and continuously available sets of array data in the world.

2. Data and Methods

[6] We obtained data for this study using the Automatic Data Request Manager (AutoDRM) of the Canadian National Data Center (CNDC). This service is remarkably efficient and large amounts of data can be obtained quickly. For each day from 1 January 1991 through 31 December 2007 we ordered one 5-minute-long segment of data from the 18 short-period seismometers at YKA. The start times were assigned using a random number generator and occurred uniformly at all times of the day. We received usable data from 6,166 of the 6,209 requests for a success rate of 99.3%. We applied an algorithm that eliminated null traces and were left with an average of 17.5 traces per time window. We did not visually inspect every trace, but we did make approximately 100 spot checks of the waveforms and found little evidence for electronic noise or data dropouts. The potential influence of transient signals from earthquakes and mining blasts is discussed later.

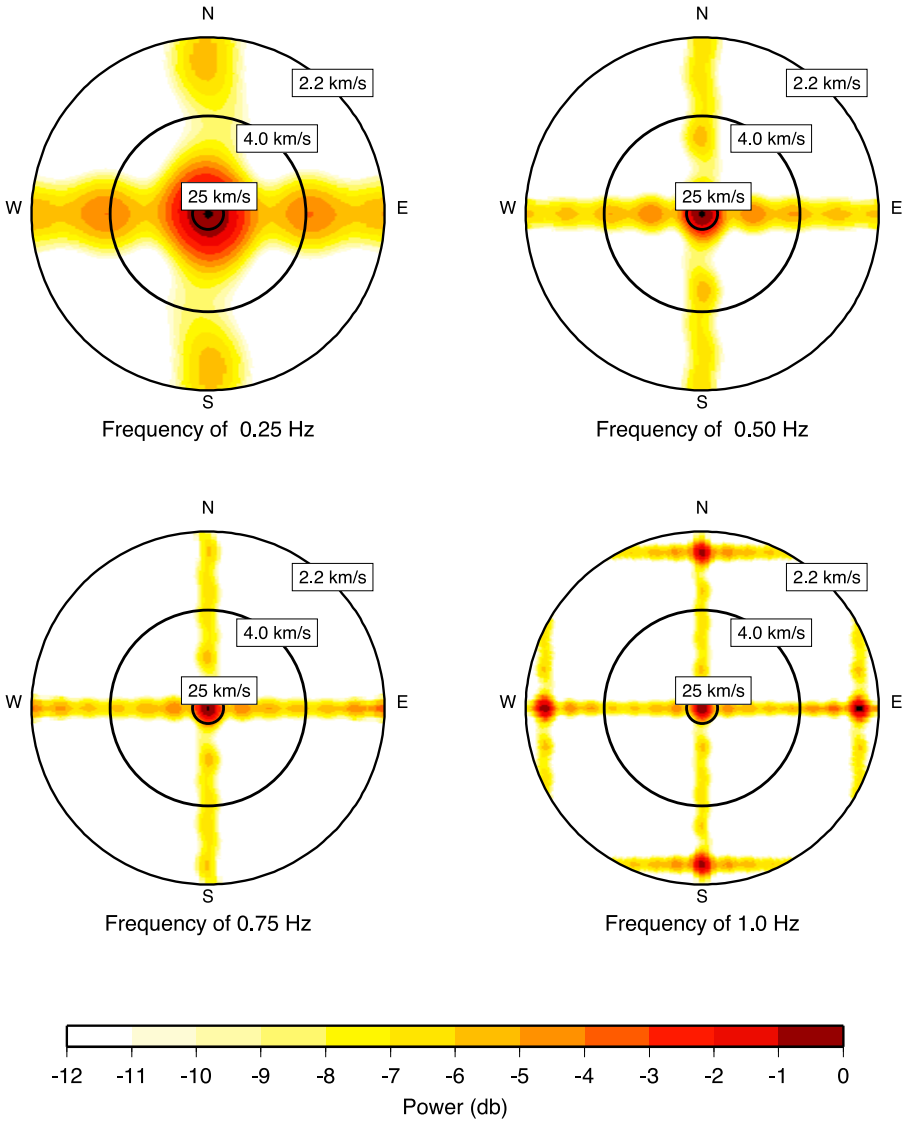

Figure 2. The slowness response of YKA to a vertically incident wave at frequencies of 0.25 Hz, 0.50 Hz, 0.75 Hz, and 1.0 Hz. An ideal array would give a single delta function at the origin. The outer radius of each panel is 50 s/deg (2.2 km/s), which is the same dimension used in the noise analysis. Note the poor resolution at low frequency (0.25 Hz) and the tiling at high frequency (1.0 Hz).

[7] The spatial arrangement of the Yellowknife array elements (Figure 1) has a profound effect on slowness resolution. The interelement spacing, $\Delta x \sim 2.5$ km, is relatively constant and is similar for both arms of the array. This leads to Nyquist wave numbers of 0.2 km^{-1} for east-west and north-south directions. Hence at a frequency of 1.0 Hz, for instance, unique information is available only within the slowness square bounded by values of ±5 s/km. When viewing the slowness field outside of this principal Nyquist square, the fundamental cross-shaped pattern of sidelobes is tiled across slowness space (Figure 2). Alternatively, low-slowness energy arriving at YKA outside of the Nyquist square can be aliased into a false higher-slowness peak within the square. In practice, this means that when analyzing a fixed region of slowness space care must be taken at higher frequencies that aliased (sidelobe) energy is not interpreted as true (mainlobe) energy.

[8] The usefulness of YKA as an array is also limited on the opposite (low) end of frequency by decreased slowness resolution. At a frequency of 0.25 Hz aliasing is not a problem but the main lobe of the response is quite broad, taking about 5–6 s/deg to decay to half-power (Figure 2). This causes a decrease in the precision of slowness estimates, and can sometimes cause peaks from two plane waves incident in the same time window to smear into one apparent peak with a slowness maximum in between the two true slownesses [e.g., *Shumway et al.*, 2008]. Because of this problem, and the aliasing problem mentioned above, we focused on frequencies between 0.25 and 0.75 Hz in the square of slowness space defined by ±50 s/deg. This yields a maximum wave number of 0.34 km^{-1}, which is above the Nyquist wave number, however, as we show later, the aliasing that results is mild and tolerable given the increase in resolution that is obtained.

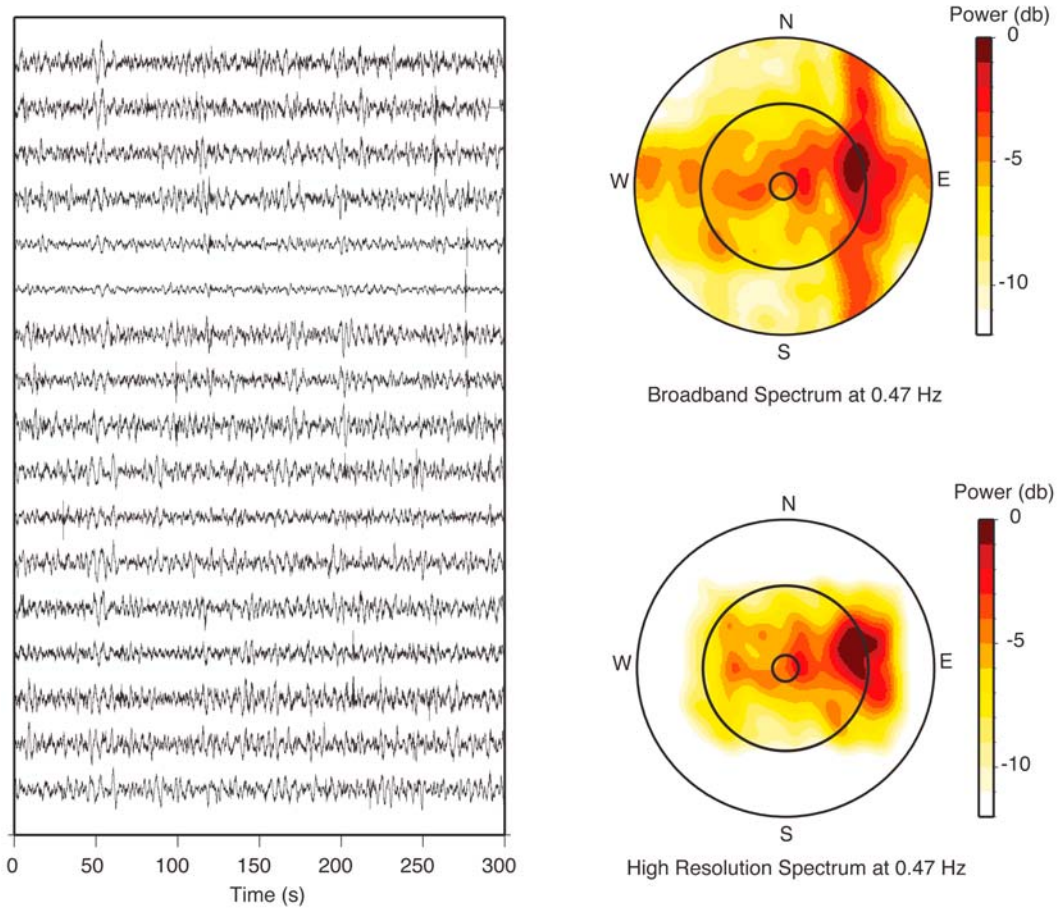

Figure 3. Example seismograms and f-k spectra for a 300 s long noise sample that began 10 January 2003 at 07:00:51 GMT. (top right) The broadband spectrum was calculated using the conventional approach and averaged over frequencies of 0.39–55 Hz, while (bottom right) the high-resolution spectrum was calculated using the approach of *Capon* [1969] but with no explicit averaging in frequency. The radii of the circles in the spectra are the same as in Figure 2, corresponding to apparent velocities of 2.2, 4.0, and 25 km/s.

[9] We used two slightly different frequency domain methods to calculate frequency-wave number (f-k) spectra. Both average heavily over time and are more appropriate for diffuse stationary signals such as microseisms as opposed to localized transient signals such as earthquake-generated body waves. In the first method we divided each noise sample into 10 nonoverlapping subwindows of length 25.6 s (512 points). For each subwindow we removed the mean, applied a Hanning taper, and calculated a Fast Fourier Transform (FFT). An overall spectral matrix for the noise sample was defined by averaging over the ten subwindows and the five nearest frequency indices. For example, the spectral matrix at a frequency of 0.31 Hz was calculated as the average of the five spectral matrices at 0.23 Hz, 0.27 Hz, 0.31 Hz, 0.35 Hz, and 0.39 Hz, averaged over the ten subwindows. Each element of this matrix, S_{jl}, was normalized by $\sqrt{S_{jj}S_{ll}}$ and the corresponding power spectrum was calculated across a uniform Cartesian slowness grid with bounds of ±50 s/deg and increments of 0.5 s/deg.

[10] In the second method we calculated f-k spectra using the high-resolution approach of *Capon* [1969]. This algorithm applies station weights that are derived to minimize the effect of the array response on the f-k spectrum. The weights are related to the inverse of the spectral matrix and so it is important that this matrix is nonsingular. To ensure this, we reduced the size of the subwindow to 6.4 s (128 points) and averaged over 40 subwindows. Because the frequency interval was increased by a factor of four compared to the first method, we did not explicitly average the spectral matrices over frequency. The power spectra were calculated using the same slowness grid as before.

[11] In Figure 3 we present seismograms from a typical noise window and the corresponding spectra for the two approaches. Although there is no obvious signal in the waveforms, both methods reveal that the energy is organized and clearly arrives from a preferred direction. The two spectra are similar with the broadband f-k estimate having maximum power at a backazimuth of 74°N and an apparent velocity of 4.5 km/s, and the high-resolution method having values of 72°N and 5.0 km/s respectively. The cross shape of the YKA response is clearly evident in the broadband estimate, while the high-resolution method does a fine job of removing this pattern and sharpening the main peak. For comparison, in Figure 4 we show f–k spectra for time windows that include energy from an earthquake that occurred to the southwest of YKA at a distance of

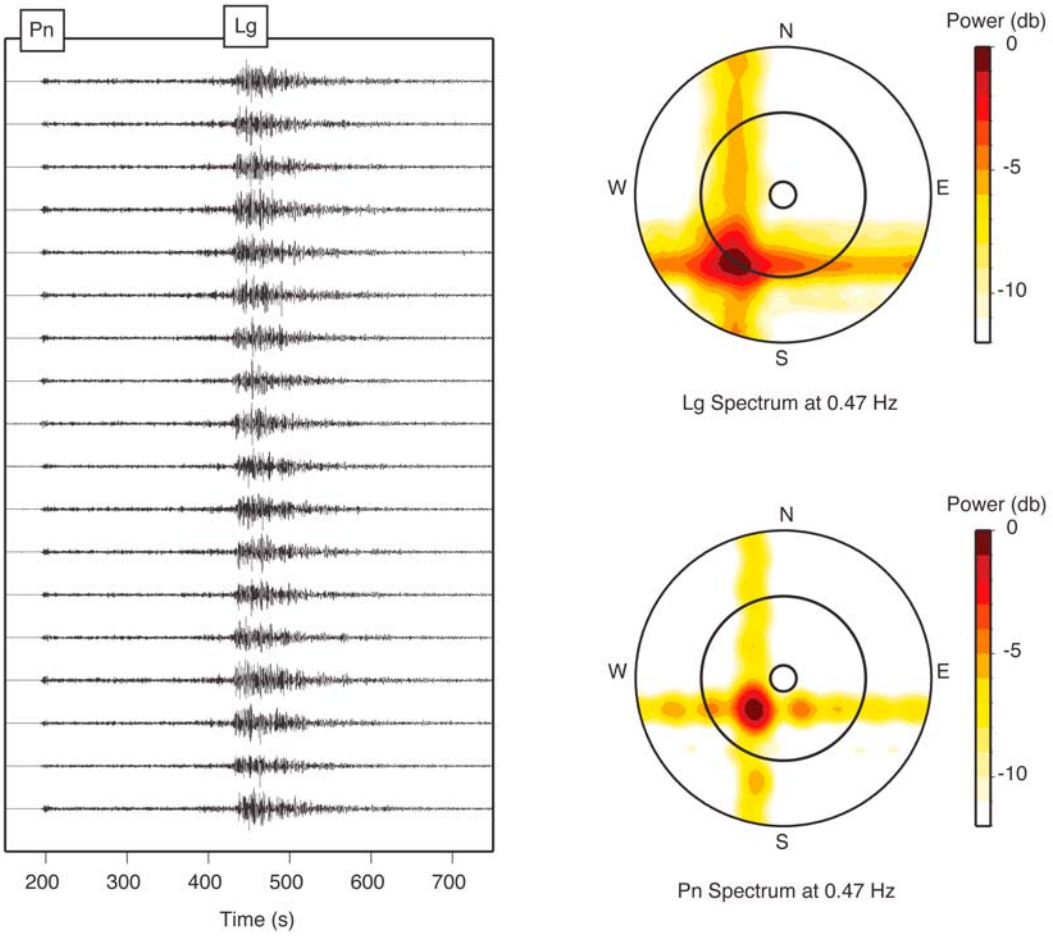

Figure 4. Example seismograms and f-k spectra for a 5.8 m_b event that occurred 12 December 2007 off the coast of British Columbia. The expected distance and backazimuth are 13.8° and 229°N, respectively. Time is relative to the origin time, and the bounds used for calculating the Lg spectrum were 420–676 s and those used for P_n were 180–282 s. Conventional f-k estimates are shown averaged over frequencies of 0.39–0.55 Hz and 4 (P_n) and 10 (L_g) subwindows of length 25.6 s. The radii of the circles in the spectra are the same as in Figures 2 and 3, corresponding to apparent velocities of 2.2, 4.0, and 25 km/s.

1,500 km. Since the earthquake energy is so coherent the spectral matrices are effectively singular and we cannot calculate the weights for the high-resolution technique without some sort of regularization. Nevertheless, the broadband method works well and gives sharper peaks when compared to the noise window (Figure 3). The time window that includes L_g and its coda has an apparent velocity of 4.0 km/s and backazimuth of 215°N, while the time window that includes P_n and its coda has an apparent velocity of 7.7 km/s and backazimuth of 224°N.

3. Composition of the YKA Noise Field

[12] There are several robust wave number peaks in the YKA noise field, reflecting a rich variety of organized noise sources over the time period of 1991–2007. We illustrate this in Figure 5 by showing two-dimensional histograms of peak slowness values. For each of the 6,166 samples of noise we determined the slowness vector with the largest power for a given frequency band and spectral method, and then incremented the corresponding 1 × 1 s/deg bin. We also experimented with two-dimensional stacking of full f-k spectra but found that the histogram presentation gave a clearer picture of the major noise sources at YKA. We note that at the highest frequency band centered on 0.62 Hz some artifacts related to spatial aliasing are visible; these are labeled with an "A" and do not reflect actual sources of noise.

[13] The influence of earthquakes in Figure 5 is negligible because of the extensive time averaging in the spectral estimation techniques and the large number of noise samples that contribute to it. We illustrate this by examining the maximum power on the normalized slowness grid for each noise sample. This value has a theoretical maximum of one for a perfectly coherent plane wave [*Capon*, 1969]. Considering the earthquake energy shown in Figure 4, the normalized power for the relatively diffuse L_g window is 0.41, while the more coherent P_n window has a value of 0.76. At the same frequencies, the 6,166 noise samples presented in Figure 5 have a mean normalized power of 0.23 ± 0.11, where the quoted error bounds are 2σ. Furthermore, we recalculated the histogram using samples

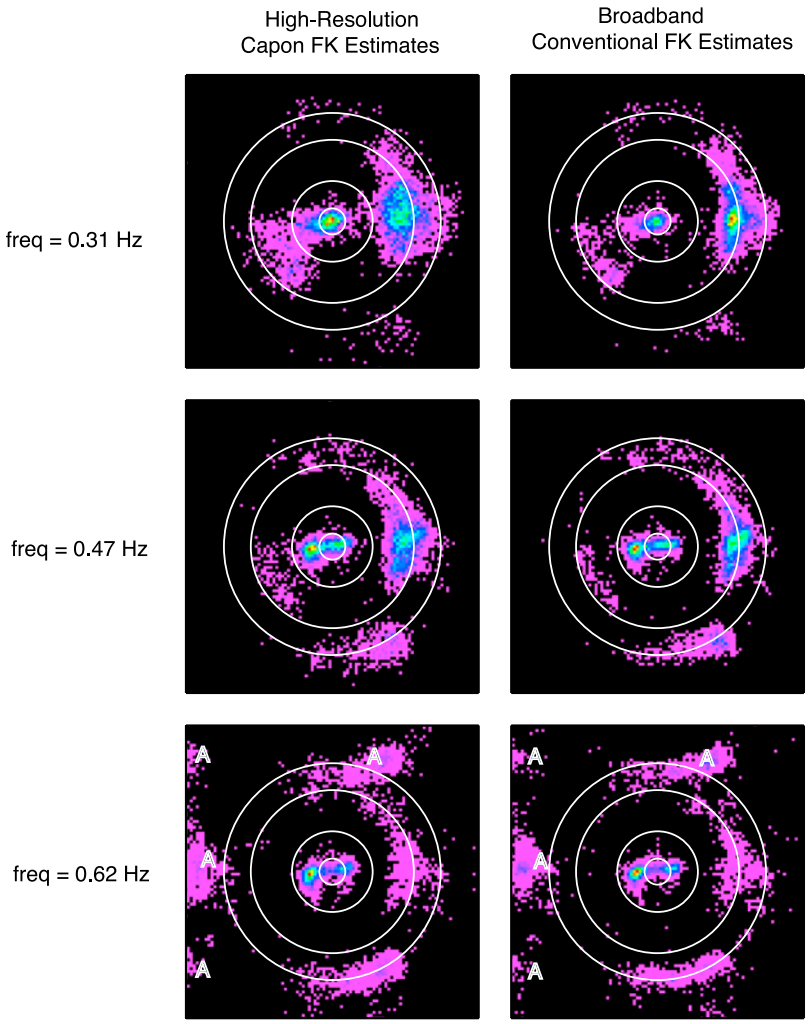

Figure 5. Histograms of maxima from the f-k spectra, binned in boxes of 1 × 1 s/deg. Each panel is individually normalized with red being highest, purple lowest, and black representing an empty bin. The panels each cover the complete search area in slowness space and have dimensions of ±50 s/deg (2.2 km/s). The circles are drawn at radii of 25, 8.1, 4.0, and 3.0 km/s, which correspond to apparent velocities of P_{diff}, P_n, L_g, and R_g, respectively. The A's in the bottom two panels indicate artifacts related to spatial aliasing.

with normalized power less than 0.3 and found the same patterns as shown in Figure 5. Clearly, the noise energy is very diffuse and has little bias from earthquakes.

3.1. The L_g Component of Noise

[14] One of the most frequently observed noise sources at YKA arrives with apparent velocities around 4.0 km/s (Figure 5). These velocities are similar to those observed for the L_g phase presented in Figure 4 as well as other earthquake-generated L_g phase velocities observed at YKA and related arrays [*Der et al.*, 1984]. They are also consistent with numerical simulations of L_g in realistic Earth models [*He et al.*, 2008]. Consequently, we infer that this energy consists of L_g waves and refer to it as such in the remainder of this paper. Since L_g is generally the dominant arrival on earthquake seismograms at short periods and regional distances, it is not surprising that it is a dominant component in the short-period noise at YKA. It was also found to be the dominant component of short-period noise at a medium aperture array in Thailand [*Koper and de Foy*, 2008].

[15] The azimuthal distribution of L_g noise energy recorded at YKA is highly correlated with the distance to the nearest coastline (Figure 6). Energy preferentially arrives from the east and to a lesser extent from the southwest and north. The two major directional gaps in L_g energy correspond to the Alaskan landmass to the northwest (270–330°N) and the main North American landmass to the south (120–210°N). The southeastern arrivals in Figure 5 have velocities around 3.0 km/s, which is too low for L_g, and are discussed in the following section.

[16] Because L_g does not propagate efficiently across ocean-continent boundaries, the L_g noise recorded at YKA is created at coastlines and not in deep water. We interpret the southwestern L_g peak as being generated by wave action in the Pacific Ocean along the coast of British Columbia and the Alaska Panhandle. Rayleigh wave microseisms from this area have been observed at longer periods at a seismic

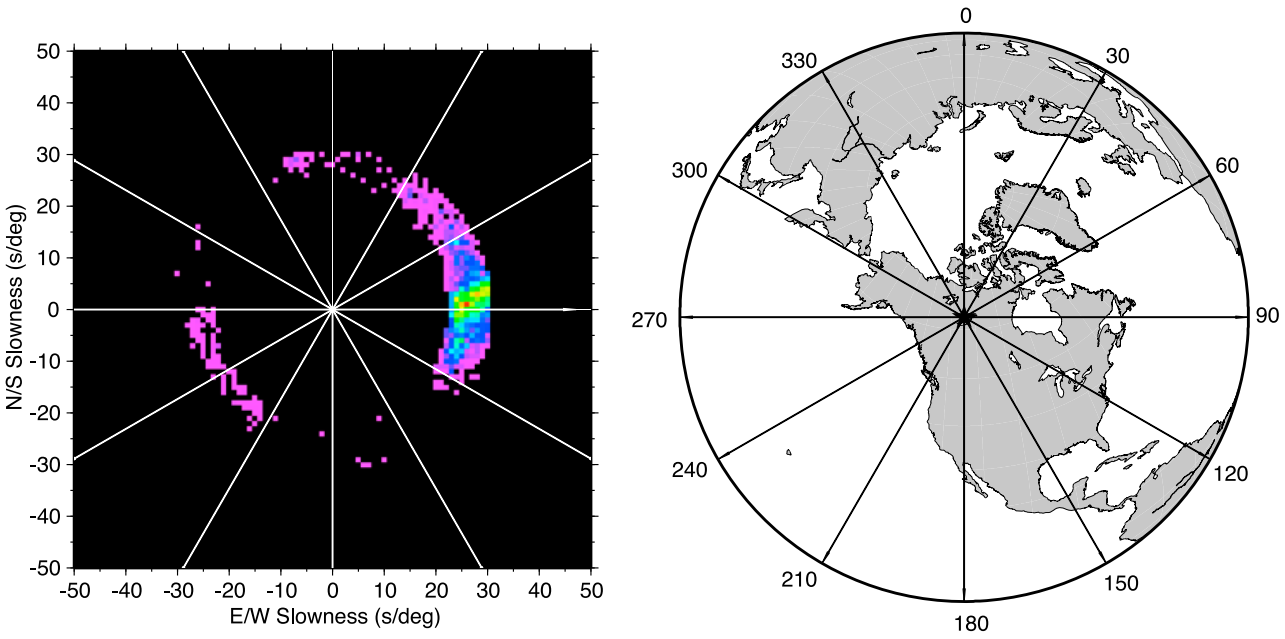

Figure 6. Comparison of f-k maxima from the broadband conventional procedure at a center frequency of 0.47 Hz (the middle right panel in Figure 5) with an orthographic map projection centered on YKA. This projection gives true angular directions (backazimuths) from the center that can be directly compared to directions in slowness space. In order to highlight the L_g energy, only f-k maxima with velocities between 3.6 and 5.0 km/s are shown.

array in southern California [*Schulte-Pelkum et al.*, 2004]. Likewise, the northern L_g arrivals are generated by wave action in the Arctic ocean along the northern coast of Alaska, Yukon, and the Northwest Territories. The dominant eastern peak is more problematic to interpret because there are two large bodies of water in that direction: Hudson Bay and the Atlantic Ocean. It is likely that the major source is the North Atlantic because waves and swell will be largest there, and because the Hudson Bay is frozen a large part of the year. The North Atlantic is well known for large waves during the winter and microseisms are commonly observed to emanate from this region [see *Kedar et al.*, 2008, and references therein].

3.2. The R_g Component of Noise

[17] The low-velocity cluster of arrivals from the southeast have velocities centered at 3.0 km/s, significantly slower than the L_g waves from other directions (Figure 5). Some azimuthal variability in L_g phase velocity is expected because of anisotropy and three-dimensional site effects, but a 25% reduction seems too large to be explained in this manner. We verified this by calculating L_g phase velocities for the 5.7 M_w Texas earthquake of 14 April 1995. This event occurred in a similar direction as the 3.0 km/s noise, with a backazimuth of 162°N, and although it was located at a distance of 33° it produced a large L_g wave train at YKA. We bounded the L_g energy using group velocities of 3.6 km/s and 3.0 km/s and observed phase velocities around 4.0 km/s, similar to what was found for the earthquake generated L_g waves shown in Figure 4.

[18] Because of the low velocity of the southeast arrivals we infer they are R_g waves as opposed to L_g. R_g waves are commonly observed for shallow sources at local and regional distances and can have large amplitude. A previous study of R_g arrivals at YKA from shallow earthquakes and mining explosions found nearly constant R_g phase velocities of 3.0–3.1 km/s at frequencies of 0.4–2.0 Hz [*Ruud et al.*, 1993]. This matches our noise observations perfectly. Owing to the high attenuation of R_g the source region for these arrivals must be nearby, and the obvious choice is the Great Slave Lake which is just a few kilometers south of YKA (Figure 1). Although this lake is frozen in the winter, presumably wave activity during the summer months is strong enough to create R_g arrivals at YKA and explain our observations.

[19] This interpretation is similar to the conclusions of an earlier study that was focused on the detection capabilities of YKA [*Weichert and Henger*, 1976]. In that work, the authors noticed a strong seasonal dependence to the detection threshold at YKA, with many more false alarms being generated during the summer. The authors performed a time domain slowness analyses on nine of the false alarms and found backazimuths of 144–158°N with a mean of 150°N, and apparent velocities of 2.7–3.6 km/s with a mean of 3.0 km/s. They interpreted the arrivals as surface waves generated by the Great Slave Lake and estimated a Q of 45. Although this noise has grossly different slowness properties than the teleseismic *P* waves that YKA was designed to detect, it created false alarms because it was spatially aliased into the teleseismic *P* portion of slowness space at high frequencies.

[20] The directional distribution of the R_g energy observed here and in *Weichert and Henger* [1976] is tightly clustered around a backazimuth of 150°N, even though the coastline of the Great Slave Lake extends from the northeast clockwise around to the northwest, or roughly 70–315°N in

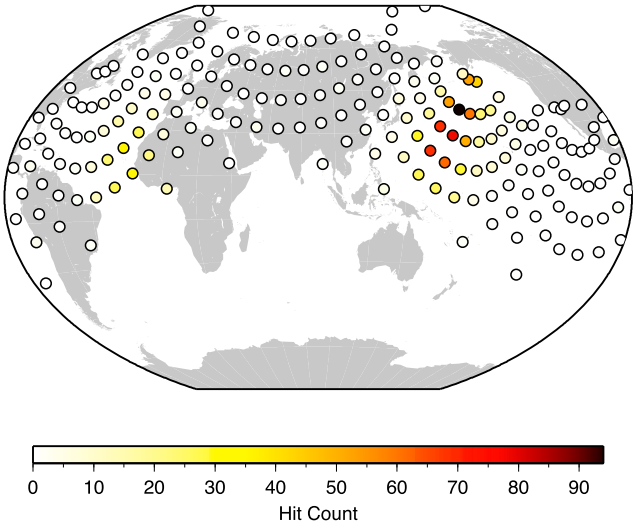

Figure 7. Backprojection of high-velocity peaks in the f-k histogram from the broadband conventional procedure at a center frequency of 0.62 Hz (the lower right panel in Figure 5). The energy is assumed to be a direct *P* wave and is propagated through AK135 assuming a surface focus. To avoid complication with upper mantle triplications and core diffractions only energy with ray parameters of 9.10–4.47 s/deg (equivalent to distances of 25–99°) is back-propagated. The wide spread in energy is partially created by relatively low slowness resolution and is not necessarily indicative of a geographically broad source region.

backazimuth (Figure 1). We speculate that the preferred direction is 150°N because this matches the strike of the coastline to the south of YKA which faces the deep central portion of the lake. The dominant frequency of the R_g waves was reported as 1.2 Hz [*Weichert and Henger*, 1976] which is much higher than the oceanic microseism band of 5–8 s and is presumably related to a shorter period for water waves in the Great Slave Lake than in the ocean. If these waves correspond to the double-frequency mechanism of wave interference proposed by *Longuet-Higgins* [1950], then the water waves on the Great Slave Lake should have a dominant period of about 1.6 s. Obviously this is testable, and we leave as future work the determination of the precise source mechanism for generating R_g waves along coast of the Great Slave Lake.

3.3. The Teleseismic *P* Component of Noise

[21] As shown in Figure 5, often the largest source of noise at YKA arrives with apparent velocities of teleseismic body waves. At low frequencies it even appears that the noise arrives with near zero slowness, implying it has interacted with Earth's core. However, we feel this is primarily an artifact related to decreased slowness resolution, because at higher frequencies two distinct peaks with teleseismic *P* velocities clearly emerge. While there may indeed be some *PKP* energy in the noise at YKA, as has been observed elsewhere [*Koper and de Foy*, 2008; *Gerstoft et al.*, 2008], the dominant body wave arrivals are teleseismic *P* waves from almost due west and due east.

[22] Unlike surface waves, with body waves it is possible to locate the corresponding source region in distance as well as in backazimuth by tracing backward through an Earth model. Some subjectivity is still involved because the observations do not constrain the depth of the source region and do not identify the phase uniquely. Here we assume that all the energy in the noise is created at the surface, and we further assume that all the energy arriving with ray parameters between 9.1 and 4.5 s/deg is a direct *P* wave corresponding to distances of 25°–99°. As a counterexample, one could assume that energy arriving with a ray parameter of 9.1 s/deg corresponds to a *PP* wave at a distance of 50°; however, *PP* is often strongly attenuated by its long upper-mantle path and is not easily observable at short periods.

[23] The results of backprojecting the body wave arrivals observed in the YKA noise is shown in Figure 7. Using data from the histogram for the broadband f-k procedure at 0.62 Hz we raytraced backward from YKA through AK135 [*Kennett et al.*, 1995]. The arrivals are concentrated exclusively in two oceanic areas: the northwest Pacific and the central Atlantic. It is remarkable how little energy corresponds to the continental areas of Eurasia, the Americas, and northern Africa, all of which are in the appropriate distance range. The only hint of continental generation for the *P* noise is on the border of west Africa; however, this is near the cutoff in distance corresponding to P_{diff} where the ray parameter flattens considerably and could in fact be related to smearing of energy generated further south near the Gulf of Guinea. This region has previously been recognized as a prolific generator of Rayleigh wave microseisms at longer periods [*Shapiro et al.*, 2006]. We note that the Pacific source region is an intraplate area that is essentially aseismic, and so these observations are conclusive evidence for ocean-wave induced teleseismic *P* waves in the deep sea.

[24] Interestingly, results similar to ours were found at YKA in a study published almost 40 years ago [*Anglin*, 1971]. In that work the author studied 99 days of continuous data in order to quantify the detection capabilities of YKA for "third zone" events, that were defined as those occurring between 30° and 90°. The authors studied the ring of slowness space between approximately 5.5 s/deg and 10 s/deg and found that the vast majority of noise triggers were associated with their regions "I" and "D", which correspond almost precisely to the north Pacific and mid Atlantic source regions we show in Figure 7. *Anglin* [1971] even found significantly more noise arrivals from the Pacific than the Atlantic, just as we do. It follows that these two regions are stable generators of microseismic *P* energy over long periods of time.

4. Time Evolution of the YKA Noise Field

[25] Simple inspection shows that the noise sources described in the previous section have clear and consistent seasonal variations. This reinforces the idea that the noise energy at YKA is created by natural, weather related processes and that there is no major tectonic or earthquake component to our observations. To examine the time variation of the YKA noise in detail we steered array beams to the major source regions identified above and analyzed beam power as a function of time. All the beams were formed using simple delay-and-sum processing on seismo-

Table 1. Properties of the Major YKA Noise Sources (1991–2007)

Noise Parameter	Slave Lake (R_g)	Atlantic (L_g)	Pacific (L_g)	Pacific (P)	Atlantic (P)
E-W Slowness (s/deg)	16.0	28.0	−24.0	−8.0	5.0
N-S Slowness (s/deg)	−32.0	0.0	−14.0	−0.5	1.0
Backazimuth (°N)	153	90	240	266	79.0
Apparent Velocity (km/s)	3.1	4.0	4.0	13.9	21.8
m_0 (dB)	1.10 ± 0.17	−1.26 ± 0.12	−3.66 ± 0.12	−1.11 ± 0.09	2.09 ± 0.09
m_1 (10^{-5} dB/day)	6.81 ± 4.84	10.0 ± 3.28	2.54 ± 3.33	0.70 ± 2.40	1.61 ± 2.54
m_2 (dB)	−5.86 ± 1.23	−2.85 ± 0.08	−1.79 ± 0.08	−1.56 ± 0.06	−2.03 ± 0.06
m_3 (dB)	1.95 ± 1.23	2.65 ± 0.08	3.51 ± 0.08	2.47 ± 0.06	1.91 ± 0.06
m_4 (dB)	−0.19 ± 1.23	−2.57 ± 0.08	−1.89 ± 0.08	−1.71 ± 0.06	−1.94 ± 0.06
m_5 (dB)	−2.37 ± 1.23	−1.50 ± 0.08	−1.35 ± 0.08	−1.16 ± 0.06	−1.21 ± 0.06
rms residual (dB)	3.48	2.36	2.40	1.73	1.82
Date of minimum	5 June	17 June	24 June	24 June	19 June
Date of maximum	12 October	23 October	2 November	29 October	22 October

grams that had been filtered between 0.3 and 0.6 Hz using a 4-pole Butterworth bandpass filter. The slowness vectors used for the five beams are listed in the top section of Table 1. Beam power was calculated as the mean square amplitude over a 60 s time window. This yielded 5 time series of length 17 years with nominal sampling intervals of 1 day.

[26] A periodogram of the Atlantic L_g time series is presented in Figure 8. Before calculating the FFT we converted all the power values to decibels relative to the median. We removed about 10 glitches presumably related to earthquakes, filled in gaps using linear interpolation, padded with zeros to reach 8192 points, and removed the mean, but we did not apply any tapers or subwindowing algorithms. There are two large peaks at periods of 1 and 0.5 years, and possibly a peak at the lowest nonzero frequency, but no other significant structure. This motivated the following six-parameter functional form for fitting the observations:

$$P(t) = m_0 + m_1 t + m_2 \sin(2\pi f_1 t) + m_3 \cos(2\pi f_1 t) + m_4 \sin(2\pi f_2 t) + m_5 \cos(2\pi f_2 t)$$

where P is the noise power in decibels relative to the median, m_i are the model parameters to be determined, f_1 is 1/365.25 day^{-1}, $f_2 = 2f_1$, and t is time in days. We defined the periodic terms in this manner, as opposed to explicit amplitude and phase, so that the inverse problem was linear and could be solved with standard least squares. The Atlantic L_g data and corresponding best fitting model are shown in Figure 9. Overall, the fit is excellent and there is little structure to the residuals. The optimal model parameters and corresponding 95% confidence intervals are listed in Table 1. The yearly component has a peak in mid-November and a trough in mid-May, while the biyearly component has peaks in early April and early October and troughs in early July and early January. Together these two components act to shorten and steepen the yearly growth of noise energy and flatten its decay. On average the quietest day of the year is 17 June and the noisiest day of the year is 23 October.

[27] The other noise sources show similar behavior with troughs in late spring/early summer and peaks in the fall, which is indicative of northern hemisphere ocean dynamics (Figure 10). Optimal model parameters and 95% confidence intervals are listed in Table 1. There is one additional

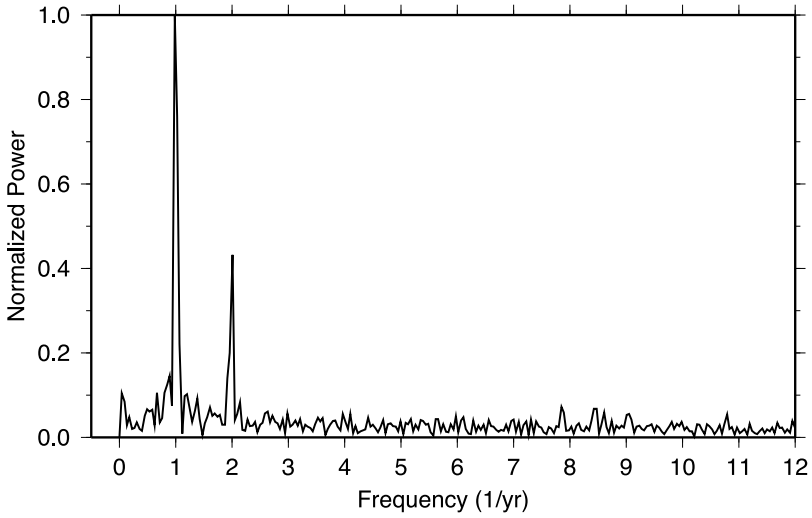

Figure 8. Periodogram of the beam power time series for the L_g noise from the Atlantic. The beam was steered due east with an apparent velocity of 4.0 km/s and the seismograms were bandpassed at 0.3–0.6 Hz with a 4-pole Butterworth filter. Prior to calculating the FFT the beam power values were converted to decibels relative to the median, the mean was removed, gaps were filled with linear interpolation, and the time series was padded with zeros to reach 8192 points.

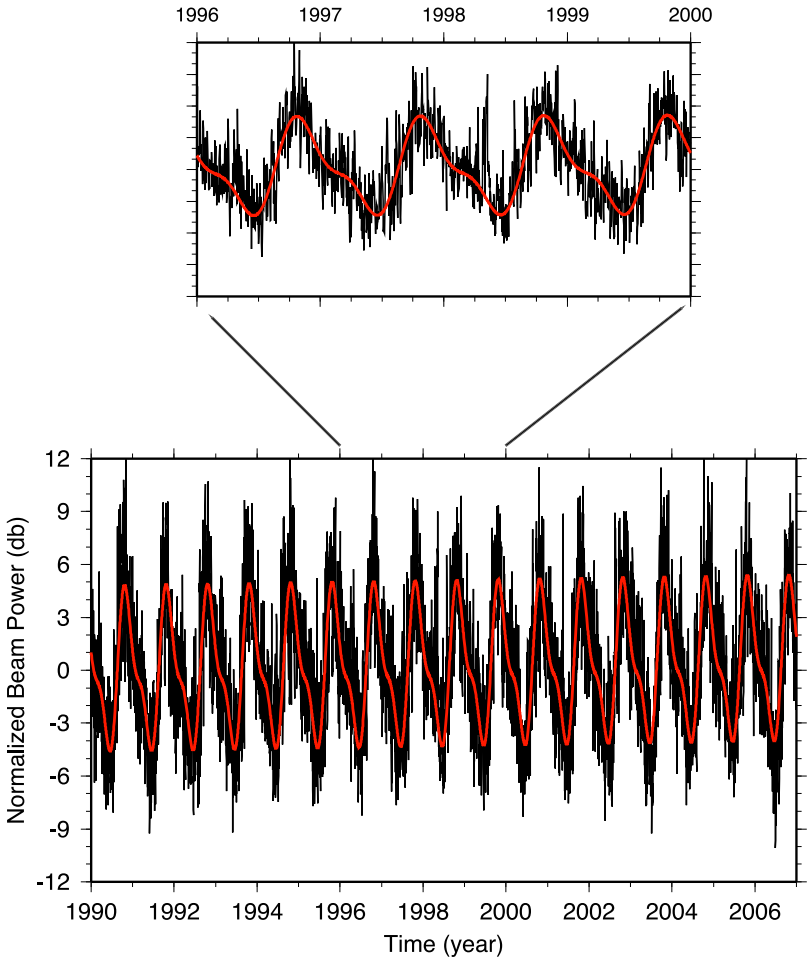

Figure 9. Power of a beam steered toward the L_g energy arriving from the east. The black curve represents the data, which are plotted as decibels relative to the median. The red curve is a least squares fit using the six-parameter model described in the text.

remarkable feature to the R_g noise from the Great Slave Lake. Most of the year this noise source is lower than the others but from summer throughfall it grows rapidly to become the most energetic source. The interesting thing is how sharp the decrease in noise level is in late fall. Over the span of about 10 days, on average from 20 November through 30 November, the noise power drops by nearly 10 dB, or roughly an order of magnitude. This is almost certainly caused by the freezing of the Great Slave Lake and the elimination of shallow lake waves. The sharpness of this drop reduces the appropriateness of the functional form given previously (higher-order Fourier terms are needed) and leads to a relatively high root-mean square residual (Table 1).

[28] The fit to the easterly L_g noise shown in Figure 9 has a positive value for m_1, the model parameter that corresponds to a linear trend in noise power. At 1.0×10^{-4} dB/day it is small, but significantly greater than zero. It corresponds to a doubling time of about 82 years. As shown in Table 1, the lower bound of the 95% confidence region is well above zero at 6.7×10^{-5} dB/day; in fact, the lower bound on the 99.9% confidence region is also well above zero at 4.5×10^{-5} dB/day and the probability of $m_1 \leq 0.0$ is less than 10^{-6}. The other noise sources also have positive m_1 values, although the only one that is significantly greater than zero is the R_g energy from the Great Slave Lake. The probability of $m_1 \leq 0.0$ in this case is about 0.003.

[29] The fact that the apparent growth in seismic noise power (as measured by m_1) is not significantly positive for all the noise sources implies that the significantly positive values for the Atlantic L_g source, and to a lesser extent the R_g source, are not being caused by a subtle change in near site geology or instrumental gain over the years 1991–2007. In those cases, we expect that the effect on apparent noise power would be independent of direction. Therefore we interpret our observations as showing increasing ocean wave activity in the North Atlantic over the last 17 years. These results are consistent with, though not directly comparable to, previous seismic noise studies that have found increasing numbers of severe, microseism-generating storms over the past 3–4 decades [*Grevemeyer et al.*, 2000; *Aster et al.*, 2008b].

5. Discussion and Conclusions

[30] Our survey of the short period noise field at the Yellowknife Seismic Array shows that at periods of 1–3 s the noise is consistently organized as propagating plane

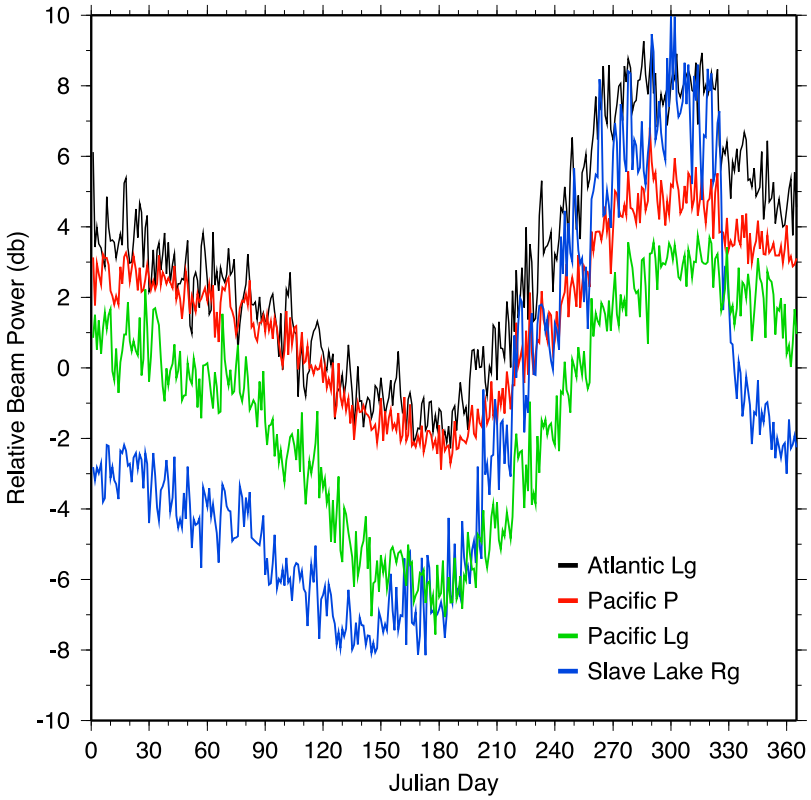

Figure 10. Annual variation in four of the noise sources observed at YKA. Each point on a curve is the median noise value for a given julian day from a beam steered toward a specific noise source. In all four cases the beams were bandpassed at 0.3–0.6 Hz with a 4-pole Butterworth filter. All of the values were normalized relative to the same level. The *P* noise from the mid-Atlantic closely tracks the *P* noise from the north Pacific and is omitted from Figure 10 for clarity.

waves. The source areas for this energy are stable over decades, and the energy itself has strong seasonal patterns. Therefore it is not being created by previously unrecognized tectonic events such as small earthquakes or tremor. At these periods it also shows no diurnal patterns and is unrelated to cultural activities such as road traffic. Instead, the noise is well correlated with the expected ocean wave climate in the northern hemisphere. Hence while the dominant global band of microseismic energy is commonly defined as 4–10 s, shorter period noise at YKA is also clearly related to natural, weather-related processes. Similar results were found in our previous work on noise at the Chiang Mai array in Thailand [*Koper and de Foy*, 2008] and these findings are consistent with the work of *Bahavar and North* [2002]. In that study the authors carried out a global survey of noise at stations of the International Monitoring System (IMS) and found that at 1 Hz nearly all noise is natural in origin and it is not until 5 Hz that the noise is obviously cultural in origin.

[31] We observed a rich variety of seismic phases in the noise at YKA including L_g, R_g, and teleseismic *P* waves. These phases are clearly distinguishable by their apparent velocities, which we found to be identical to those of corresponding earthquake-generated phases. At periods of 1–3 s the upper-crust sensitive R_g energy has velocities around 3.0 km/s and the lower-crust sensitive L_g has velocities around 4.0 km/s. The most common apparent velocity for the *P* energy is around 14 km/s, corresponding to a ray parameter of 8 s/deg and a *P* wave distance of 45°. A secondary peak in the *P* noise occurs near velocities of 22 km/s, corresponding to a ray parameter of 5.1 s/deg and *P* wave distance of 84°. There is significant smearing and scatter in slowness space for the *P* noise band and we cannot rule out the presence of *PKP* energy, as well as some regional distance (<30°) *P* energy especially from the southwest.

[32] R_g waves have high attenuation and it is because YKA is so close to the Great Slave Lake that they are observable in the noise. Earlier observations of this noise source at YKA estimated a Q of 45 [*Weichert and Henger*, 1976]. Shallow action in the lake is likely responsible for the R_g waves and it is remarkable that they travel as a plane wave across the array since they are generated so near by. Most of the year the R_g noise is the quietest component at YKA, however in late summer and fall it grows dramatically to become the largest component. The dropoff in R_g energy in late fall is even more dramatic and over the course of about 10 days (on average 20–30 November) its power drops by an order of magnitude. Such a sharp drop is not seen in the other noise components and we attribute it to the freezing of the Great Slave Lake.

[33] The most commonly observed noise propagation mode at YKA is L_g. We found that its strength is not isotropic and that it strongly depends on backazimuth. It is well observed to the east, being generated mainly along the northeastern coast of North America (Atlantic Ocean), and

to a lesser extent from the southwest (Pacific Ocean) and the north (Arctic Ocean). It is blocked from the northwest by Alaska and blocked from the south/southeast by North America. Because L_g does not propagate across ocean-continent margins, its source must be along the relevant portions of coastline and not in deep water. The L_g energy created along the North Atlantic coastline has been systematically increasing in strength over the last 17 years, implying increasing ocean wave activity in this region.

[34] Based on the observations reported here, those made in our previous work at the Chiang Mai array in Thailand [*Koper and de Foy*, 2008], and a preliminary f-k analysis of yearlong segments of data from 18 IMS array stations (K. D. Koper et al., On the composition of Earth's short period seismic noise field, submitted to *Bulletin of the Seismological Society of America*, 2009), it seems that L_g is the dominant component in Earth's short period noise field. This is perhaps not surprising since L_g is often the dominant component in short-period earthquake seismograms. It is intriguing though, because L_g is composed of shear waves trapped in Earth's crust and it is not obvious how the fluid oceans impart so much shear energy to the solid Earth. An analogous situation exists with the recent observation of significant torsional energy in Earth's long-period background noise [*Kurrle and Widmer-Schnidrig*, 2008; *Tanimoto*, 2008].

[35] In contrast to the surface wave noise, the *P* noise at YKA is generated in deep water away from coastlines. The westerly *P* noise in particular is well resolved to occur in the nearly aseismic north central Pacific Ocean. The most frequent source location is approximately 40°N 180°W, about 1,300 km south of the nearest plate boundary (the Aleutian trench) with water depths over 5 km. Most likely this energy is created by an effect in which opposing trains of ocean waves create a standing wave in which the pressure perturbation does not decay with depth [*Longuet-Higgins*, 1950]. The forcing on the ocean floor is proportional to the product of the heights of the two interfering ocean waves, which in the stormy North Pacific is presumably large enough to generate teleseismic *P* energy. Future work will be to verify the viability of this mechanism with synthetic seismograms, similar to the approach *Kedar et al.* [2008] used in simulating surface wave microseisms in the North Atlantic.

[36] In conclusion, our observation of a stable, consistent source of 1–2 s *P* waves in the north Pacific has implications for imaging Earth's mantle. Similar to imaging the crust with ambient surface wave noise, it may be possible to image Earth's mantle under the Pacific using teleseismic Green's functions derived from cross-correlating seismograms from stations around the North Pacific. This region is severely undersampled by direct *P* waves and tomographers in general have to rely on less-precise later arriving phases such as *PP* to image the upper and midmantle structure beneath the Pacific [e.g., *Lei and Zhao*, 2006]. If high-quality *P* wave Greens functions are retrievable from the north Pacific microseismic source identified here, then significantly improved tomograms of this region can be expected.

[37] **Acknowledgments.** The work presented here was partially supported by the U.S. Air Force Research Laboratory under contract FA871806C0003. During the writing of this manuscript K.D.K. was hosted and supported by the National Earthquake Information Center (NEIC) of the United States Geological Survey (USGS). We thank Sebastian Rost and Charles Langston for critical comments on this work.

References

Anglin, F. M. (1971), Detection capabilities of the Yellowknife seismic array and regional seismicity, *Bull. Seismol. Soc. Am.*, *61*, 993–1008.

Aster, R. C., D. E. McNamara, and P. D. Bromirski (2008a), Multidecadal climate-induced variability in microseisms, *Seismol. Res. Lett.*, *79*, 194–202.

Aster, R. C., D. E. McNamara, P. D. Bromirski, L. Gee, and C. R. Hutt (2008b), Microseism-based climate monitoring (abstract), *Seismol. Res. Lett.*, *79*, 306.

Bahavar, M., and R. North (2002), Estimation of background noise for International Monitoring System seismic stations, *Pure Appl. Geophys.*, *159*, 911–944.

Bondar, I., R. G. North, and G. Beall (1999), Teleseismic slowness-azimuth station corrections for the International Monitoring System seismic network, *Bull. Seismol. Soc. Am.*, *89*, 989–1003.

Bromirski, P. D. (2001), Vibrations from the perfect storm, *Geochem. Geophys. Geosyst.*, *2*(7), 1030, doi:10.1029/2000GC000119.

Bromirski, P. D., R. E. Flick, and N. Graham (1999), Ocean wave height determined from inland seismometer data: Implications for investigating wave climate changes in NE Pacific, *J. Geophys. Res.*, *104*(C9), 20,753–20,766.

Bromirski, P. D., F. K. Duennbier, and R. A. Stephen (2005), Mid-ocean microseisms, *Geochem. Geophys. Geosyst.*, *6*, Q04009, doi:10.1029/2004GC000768.

Capon, J. (1969), High-resolution frequency-wavenumber spectrum analysis, *Proc. IEEE*, *57*, 1408–1418.

Cessaro, R. K. (1994), Sources of primary and secondary microseisms, *Bull. Seismol. Soc. Am.*, *84*, 142–148.

Chevrot, S., M. Sylvander, S. Benahmed, C. Ponsolles, J. M. Lefevre, and D. Paradis (2007), Source locations of secondary microseisms in western Europe: Evidence for both coastal and pelagic sources, *J. Geophys. Res.*, *112*, B11301, doi:10.1029/2007JB005059.

Courtland, R. (2008), Earth science: Harnessing the hum, *Nature*, *453*, 146–148.

Der, Z., M. E. Marshall, A. O'Donnell, and T. W. McElfresh (1984), Spatial coherence structure and attenuation of the Lg phase, site effects, and interpretation of the Lg coda, *Bull. Seismol. Soc. Am.*, *74*, 1125–1147.

Friedrich, A., F. Kruger, and K. Klinge (1998), Ocean-generated microseismic noise located with the Gräfenberg array, *J. Seismol.*, *2*, 47–64.

Gerstoft, P., M. C. Fehler, and K. G. Sabra (2006), When Katrina hit California, *Geophys. Res. Lett.*, *33*, L17308, doi:10.1029/2006GL027270.

Gerstoft, P., P. M. Shearer, N. Harmon, and J. Zhang (2008), Gloabl P, PP, and PKP microseisms observed from distant storms, *Geophys. Res. Lett.*, *35*, L23306, doi:10.1029/2008GL036111.

Grevemeyer, I., R. Herber, and H. Essen (2000), Microseismological evidence for a changing wave climate in the northeast Atlantic Ocean, *Nature*, *408*, 349–352.

Haubrich, R. A., and K. McCamy (1969), Microseisms: Coastal and pelagic sources, *Rev. Geophys.*, *7*, 539–571.

He, Y., X.-B. Xie, and T. Lay (2008), Explosion-source energy partitioning and Lg-Wave excitation: Contributions of free-surface scattering, *Bull. Seismol. Soc. Am.*, *98*, 778–792.

Kedar, S., M. Longuet-Higgins, F. Webb, N. Graham, R. Clayton, and C. Jones (2008), The origin of deep ocean microseisms in the North Atlantic Ocean, *Proc. R. Soc., Ser. A*, *464*, 777–793.

Kennett, B. L. N., E. R. Engdahl, and R. Buland (1995), Constraints on seismic velocities in the Earth from travel times, *Geophys. J. Int.*, *122*, 108–124.

Koper, K. D., and B. de Foy (2008), Seasonal anisotropy in short-period seismic noise recorded in South Asia, *Bull. Seismol. Soc. Am.*, *98*, 3033–3045.

Kurrle, D., and R. Widmer-Schnidrig (2008), The horizontal hum of the Earth: A global background of spheroidal and toroidal modes, *Geophys. Res. Lett.*, *35*, L06304, doi:10.1029/2007GL033125.

Lei, J., and D. Zhao (2006), Global P-wave tomography: On the effect of various mantle and core phases, *Phys. Earth Planet. Inter.*, *154*, 44–69.

Longuet-Higgins, M. (1950), A theory of the origin of microseisms, *Philos. Trans. R. Soc. London, Ser. A*, *243*, 1–35.

Ruud, B. O., E. S. Husebye, and S. O. Hestholm (1993), Rg observations from four continents: Inverse- and forward-modelling experiments, *Geophys. J. Int.*, *114*, 465–472.

Sabra, K. G., P. Gerstoft, P. Roux, W. A. Kuperman, and M. C. Fehler (2005), Surface wave tomography from microseisms in Southern California, *Geophys. Res. Lett.*, *32*, L14311, doi:10.1029/2005GL023155.

Schulte-Pelkum, V., P. S. Earle, and F. L. Vernon (2004), Strong directivity of ocean-generated seismic noise, *Geochem. Geophys. Geosyst.*, *5*, Q03004, doi:10.1029/2003GC000520.

Shapiro, N. M., M. Campillo, L. Stehly, and M. H. Ritzwoller (2005), High-resolution surface-wave tomography from ambient seismic noise, *Science*, *307*, 1615–1618.

Shapiro, N. M., M. H. Ritzwoller, and G. D. Bensen (2006), Source location of the 26 sec microseism from cross-correlations of ambient seismic noise, *Geophys. Res. Lett.*, *33*, L18310, doi:10.1029/2006GL027010.

Shumway, R. H., E. Smart, and D. A. Clauter (2008), Mixed signal processing for regional and teleseismic arrays, *Bull. Seismol. Soc. Am.*, *98*, 36–51.

Stehly, L., M. Campillo, and N. M. Shapiro (2006), A study of the seismic noise from its long-range correlation properties, *J. Geophys. Res.*, *111*, B10306, doi:10.1029/2005JB004237.

Tanimoto, T. (2008), Geophysics: Humming a different tune, *Nature*, *452*, 539–541.

Weichert, D. H., and M. Henger (1976), The Canadian seismic array monitor processing system (CANSAM), *Bull. Seismol. Soc. Am.*, *66*, 1381–1403.

Yang, Y., and M. H. Ritzwoller (2008), The characteristics of ambient seismic noise as a source for surface wave tomography, *Geochem. Geophys. Geosyst.*, *9*(2), Q02008, doi:10.1029/2007GC001814.

H. Benz, National Earthquake Information Center, United States Geological Survey, Box 25046, MS966, Denver, CO 80225, USA. (benz@usgs.gov)

B. de Foy and K. D. Koper, Department of Earth and Atmospheric Sciences, Saint Louis University, 3642 Lindell Boulevard, St. Louis, MO 63108, USA. (bdefoy@slu.edu; kkoper@gmail.com)